

Article

Synthesis and Characterization of Ch-PANI-Fe₂O₃ Nanocomposite and Its Water Remediation Applications

Bharatraj Singh Rathore ¹, Narendra Pal Singh Chauhan ^{2,*}, Perumal Panneerselvam ³, Sapana Jadoun ⁴, Mahmood Barani ^{5,*}, Suresh C. Ameta ^{6,†} and Rakshit Ameta ⁷

¹ Department of Chemistry, Vidya Bhawan Rural Institute, Udaipur 313011, Rajasthan, India

² Department of Chemistry, Bhupal Nobles University, Udaipur 313002, Rajasthan, India

³ Department of Chemistry, SRM Institute of Science and Technology, Kattankulathur 603203, Tamil Nadu, India

⁴ Laboratorio de Especiación y Trazas Elementales, Departamento de Química Analítica e Inorgánica, Facultad de Ciencias Químicas, Universidad de Concepción, Concepción 4030000, Chile

⁵ Medical Mycology and Bacteriology Research Center, Kerman University of Medical Sciences, Kerman 7616913555, Iran

⁶ Department of Chemistry, PAHER University, Udaipur 313003, Rajasthan, India

⁷ Department of Chemistry, J. R. N. Rajasthan Vidyapeeth (Deemed to be University), Udaipur 313001, Rajasthan, India

* Correspondence: narendrapalsingh14@gmail.com (N.P.S.C.); mahmoodbarani7@gmail.com (M.B.)

† Dedicated to Professor Suresh C. Ameta on the occasion of his 75th birthday.

Abstract: Using the batch adsorption technique, an eco-friendly polymer composite made of chitosan, polyaniline, and iron (III) oxide was developed for removal of dye contamination from wastewater. Ultraviolet-visible spectroscopy (UV-Vis), Fourier transform infrared spectroscopy (FTIR), scanning electron microscopy (SEM), X-ray diffraction (XRD), transmission electron microscopy (TEM), EDX (energy dispersive X-ray analysis), and thermogravimetric-derived thermogravimetric (TG-DTG) techniques were used to characterize the sample. According to EDX, the Ch-PANI-Fe₂O₃ hybrid composite has the following weight ratios: C 34.25%, N 0.48%, O 50.51%, and Fe 3.08%. The nanocomposite's surface was rough with pleats, which was evident from the SEM and TEM images. This surface structure likely contributed to the nanocomposite's higher dye adsorption rate (91.5%). According to SEM analysis, the proportion of Fe₂O₃ nanoparticles to the chitosan–polyaniline composite changed the hybrids' morphology from granular to an irregular, globular-like structure, which was supported by EDX. The results demonstrated that this polymer matrix (chitosan-PANI-Fe₂O₃) nanocomposite can be employed as an adsorbent for the effective removal of methyl orange dye, as well as for the removal of dye contamination from wastewater with reusability.

Keywords: composite; chitosan; polyaniline; Fe₂O₃ NPs; adsorption; methyl orange; wastewater



Citation: Singh Rathore, B.; Pal Singh Chauhan, N.; Panneerselvam, P.; Jadoun, S.; Barani, M.; Ameta, S.C.; Ameta, R. Synthesis and Characterization of Ch-PANI-Fe₂O₃ Nanocomposite and Its Water Remediation Applications. *Water* **2022**, *14*, 3615. <https://doi.org/10.3390/w14223615>

Academic Editor: Constantinos V. Chrysikopoulos

Received: 1 October 2022

Accepted: 7 November 2022

Published: 10 November 2022

Publisher's Note: MDPI stays neutral with regard to jurisdictional claims in published maps and institutional affiliations.



Copyright: © 2022 by the authors. Licensee MDPI, Basel, Switzerland. This article is an open access article distributed under the terms and conditions of the Creative Commons Attribution (CC BY) license (<https://creativecommons.org/licenses/by/4.0/>).

1. Introduction

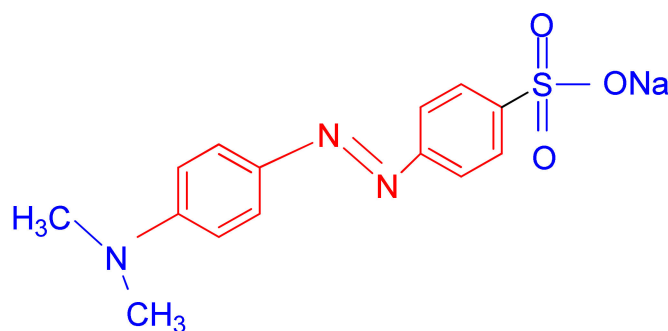
One of the most serious environmental issues today is industrial wastewater containing organic pollutants. One potential remedy is to develop an environment-friendly and efficient material to degrade the organic pollutant [1–3]. The most significant colorants, dyes and pigments, are extensively used in a variety of sectors, including textiles, inks, drugs, food, plastics, cosmetics, paints, photographs, and paper [4]. As a result, they produce large amounts of unappealing colored industrial wastewater [5,6]. Wastewater containing dyes and pigments renders it unattractive and poses significant health risks to both the environment and living organisms [7]. The printing and dyeing industries have recently undergone rapid innovation, which has greatly improved peoples' quality of life [8]. However, this industry's wastewater has also contributed significantly to water pollution, endangering the advancement of society [9].

Nanotechnology, the manipulation of matter at a molecular or an atomic level to craft new structures, devices, and systems having superior electronic, optical, magnetic, conductive, and mechanical properties, is emerging as a promising technology, which has demonstrated remarkable feats in various fields [10,11]. Nanomaterials encompass a high surface to volume ratio, a high sensitivity and reactivity, a high adsorption capacity, and ease of functionalization [12]. Real uses of nanostructured materials in life sciences are uncommon at the present time. The excellent properties of these materials provide a very promising future for their use in this field.

Many techniques for the removal of dye contaminants have been used for a long time; however, adsorption is an efficient method for the efficient removal of pollutants from wastewater due to its simple operation, lack of by-products, and large-scale removal of contaminants [13]. Until now, numerous materials have been synthesized for the effective removal of toxic dyes from wastewater. Anuma et al. investigated the adsorption performance of a cobalt oxide graphene nanocomposite functionalized with a polypyrrole composite in a systematic manner for the removal of methylene blue, Congo red, and toxic heavy metals [14]. A polymer nanocomposite based on the amino acid proline was used by Raghunath et al. [15] for the removal of blue 222, reactive red 195, and reactive yellow 145 from industrial waste water. The carboxylated-multiwalled carbon nanotubes (MWCNTs)/polyether sulfone PESs are promising nanocomposite membranes, which exhibited favorable removal of pollutants of industrial effluents [16]. The removal of methyl red dye was also observed using polyvinyl alcohol (PVA) and a multiwalled carbon nanotube (MWCNT) composite [17]. Etaweil et al. investigated the UiO-66/MIL-101(Fe)-GO-COOH composite's adsorption capabilities [18] for its efficiency to adsorb cationic methylene blue. Magnetically recoverable cross-linked polyethylenimine (MPEI) composites were used by Chen et al. for the removal of anionic dyes in an effective manner [19]. $\text{CoFe}_{1.98}\text{Sm}_{0.02}\text{O}_4$ @chitosan-glutaraldehyde composites were employed to remove acid orange 7 from aqueous solution [20].

Conducting polymers (CPs) have the advantage of low density, chemical diversity, flexibility, corrosion resistance, easily controlled shape, morphology, and tunable conductivity as compared to their existing inorganic counter parts [21]. Among all the conducting polymers, polyaniline (PANI) has low-cost monomers, reasonably good thermal stability, and excellent biocompatibility [22,23]. Activated carbon and a CP composite were used by Supriya et al. to observe the adsorption of acid orange 7 from industrial effluents [24]. The removal of dyes from simulated industrial effluents was accomplished by Abbasian et al. using cellulose/PANI nanocomposites that were made using an in situ chemical oxidation polymerization method [25]. Polyaniline/ TiO_2 (PANI/ TiO_2) was applied by Wang et al. [26] for the adsorption of dye. A PANI/ Fe_3O_4 composite was used by Muhammad et al. [27] for the removal of acid blue 40 from an aqueous environment.

Chitosan is a natural and linear bio-polyaminosaccharide having many applications in the field of separation and food, pharmaceutical, medicine, and cosmetic industries [28]. Magnetic nanoparticles are currently the focus of intense research activities [29,30]. This is not only due to their use in practical applications, e.g., as theranostic agents in medicine or as ferrofluids in engineering technologies, but also due to their role as fundamental model systems for nanoscale phenomena [31,32]. Nano-sized metal oxide can easily remove dyes due to its large surface area and high activity [33,34]. Some recent work related to polyaniline–chitosan–metal oxide composites is tabulated in Table 1. A chemical structure of methyl orange is depicted in Scheme 1.



Scheme 1. Structure of methyl orange.

Table 1. Polyaniline–chitosan–metal oxide composites.

S. No.	Polymer Composite	Method	Properties and Applications	References
1	PANI/Ch/ZnO	Single-step in situ oxidation polymerization	Better thermal and electrical property	[35]
2	PANI/Ch/ZnO	Precipitation–oxidation method	Wastewater pollutants	[36]
3	PANI-g-Ch/Co ₃ O ₄	Oxidative radical copolymerization	Photocatalytic activity	[37]
4	PANI/Ch/ZnO	Chemical polymerization	Removal of dye	[38]
5	PANI/Ch/NiO	Chemical route and Breath Figure technique	Electrical conductivity and supercapacitor properties	[39,40]

In the current study, a nanocomposite made of biodegradable chitosan, conducting polyaniline (PANI), and iron oxide (Fe₂O₃) was developed using ammonium peroxydisulfate as an initiator in an acidic medium. The performance of the photocatalytic process was assessed by observing the adsorption of the dye methyl orange under UV irradiations.

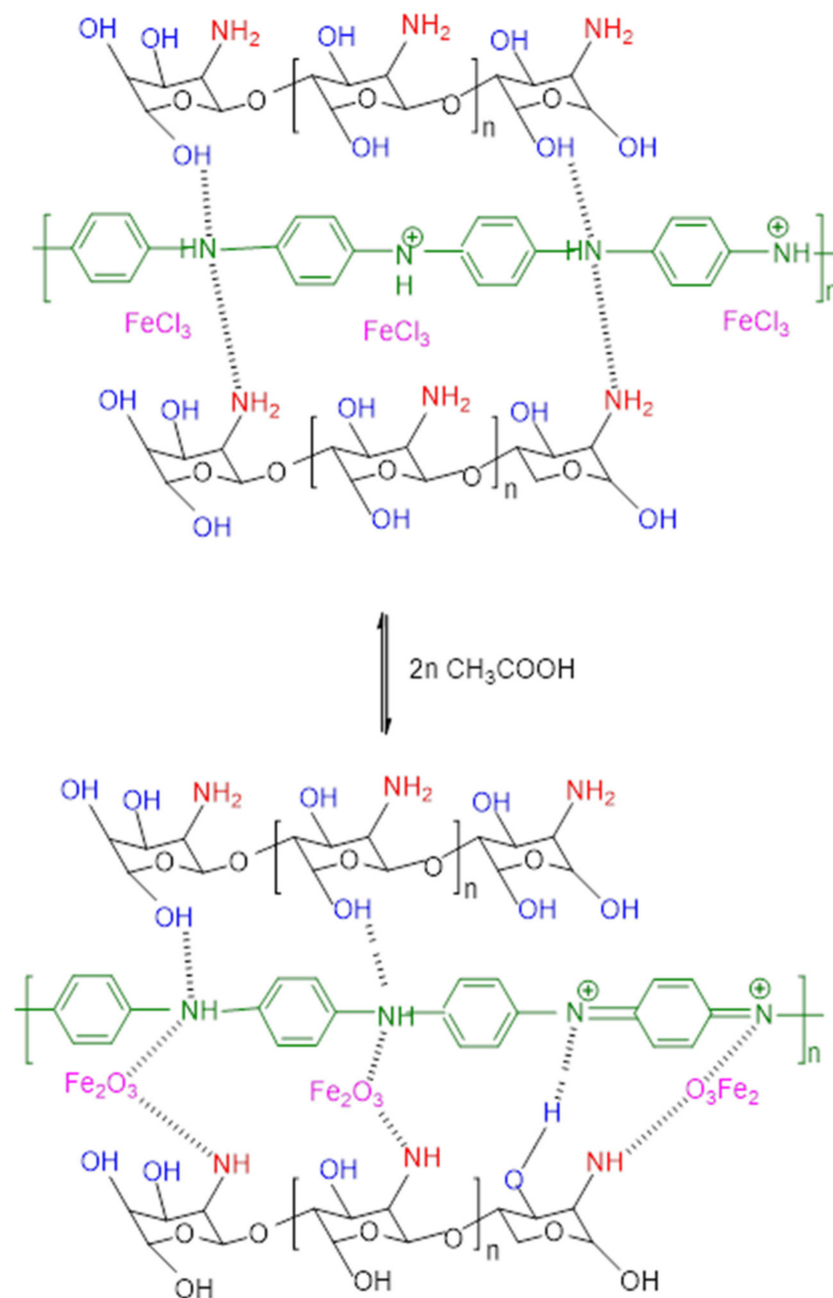
2. Materials and Methods

2.1. Materials

Purchases were made from Hi-media, India, for chitosan (75% degree of deacetylation), iron (III) oxide, ammonium persulfate (APS), and iron (III) chloride. Hydrochloric acid, sodium hydroxide, methyl orange, and aniline were purchased from Merck, India. All reagents were prepared using double distilled water. All other compounds in the experiment were made with analytical-grade chemicals.

2.2. Method

Aqueous acetic acid (20%) and 1.0 g of chitosan were combined and stirred for 24 h at 25 °C. Then, a homogeneous solution was prepared by dissolving aniline (0.01 M) in acetic acid (1.0 M) and stirring for 30 min. This solution was continuously stirred at 0 °C for 8 h with the addition of 15.0 g of ammonium peroxydisulfate that had been dissolved in acetic acid, and black-green colored precipitate was obtained which was washed with water and methanol. As a result, it lost its color. At 60 °C for 24 h, the final composite was dried. After being dissolved in 100 mL of distilled water, the 5.0 g of FeCl₃ and the 1.0 g of Fe₂O₃ were added to the polyaniline–chitosan composite. This mixture was warmed for two hours to 70 °C. A 3 h ice bath was used to cool the resulting solution. Using distilled water, the brick red precipitate was cleaned. It was subsequently washed with methanol, which made it colorless and dried at 70 °C for 18 h. The proposed framework is presented in Scheme 2. The interactions between Fe₂O₃ and polymeric chains (chitosan and PANI) may be attributed to hydrogen bonding.



Scheme 2. Proposed structure of Ch-PANI-Fe₂O₃ composite. Amino groups: red; Hydroxy groups: blue; polyaniline chain: green; chitosan chain; black; ferric chloride and ferric oxide: pink.

2.3. Characterization

Perkin Elmer's Spectrum GX range FTIR Spectrometer, which has a resolution of 0.15 cm⁻¹, was used to record the FTIR spectra. A range of 400 to 4000 cm⁻¹ of spectrum was scanned. The value of λ_{max} was ascertained using a Perkin Elmer UV VIS NIR Spectrophotometer Lambda 750 from Waltham, MA, USA. The scan rate was 20 scans per second. Monochromatic Cu K radiation (=1.5406) was used for the XRD pattern measurement, which was used to study the structures of the nanocomposite. Using a JEOL JSM-6100 microscope, scanning electron microscopy (SEM) was used to determine the morphological characteristics and surface properties of the Ch-PANI-Fe₂O₃ composite (Tokyo, Japan). Using a Philips, Holland, Model Tecnai 20 TEM, images of the Ch-PANI-Fe₂O₃ composite film were captured. A transmission electron microscope with a W emitter and LaB₆ electron source was employed at an acceleration voltage of 200 kV. It can magnify objects by

a factor of 750,000 or more using electron beam optics. Thermal analysis was performed in a nitrogen environment using a Perkin Elmer TGA apparatus (Model TGA 8000) at temperatures ranging from 50 °C to 850 °C at a heating rate of 10 °C/min. After switching to an oxygen atmosphere, the temperature range was set from 750 °C to 850 °C at the same heating rate. The energy dispersive X-Ray (EDX) detector and Carl Zeiss scanning electron microscope (SEM) were used to analyze the elements in the nanocomposite (Model EVO 18). Images were captured using 10 KV of accelerated energy and a 200× magnification.

2.4. Dye Adsorption Study

Batch experiments were performed to study the removal of dye using the method proposed by Mahanta and coworkers [41]. In a rotatory shaker, 0.1 g of the composite was individually stirred with 100 mL of dye solution at 30 °C. The shaking speed was kept constant throughout the experiment at 180 rpm. Samples were taken at the predetermined intervals, and the dye solution and adsorbent were separated using centrifugation at 6000 rpm for five minutes. In order to determine the dye concentration, a UV-Vis spectrophotometer was used to record the dyes' absorbance.

The following formula was used to determine the percentage of methyl orange removal:

$$\text{Removal (\%)} = \frac{C_i - C_e}{C_i} \times 100$$

where C_i is the starting dye concentration and C_e is the dye concentration at equilibrium in milligrams per liter. The following equation was used to calculate the maximum amount of dye that could adsorb at equilibrium:

$$q_e = (C_i - C_e) \frac{V}{M}$$

where M is the mass of the composite used, V is the solution volume, and C_i and C_e are the initial and equilibrium dye concentrations (mgL^{-1}), respectively. In order to illustrate the equilibrium time, the methyl orange (MO) dye's adsorption on the composite was studied at various initial dye concentrations, pH levels, and doses of adsorbent. It was noted that the removal of methyl orange began rapidly in the first five minutes and then gradually slowed as more time passed until equilibrium. The presence of more adsorption sites on the surface of the composite may be the cause of the initial state's increased adsorption activity. After that, as more methyl orange dye was adsorbed on the surface of the composite, the adsorption rate started to slow down.

For methyl orange, a contact period of about 45 min was necessary to reach equilibrium. According to Pandiselvi and Thambidurai, the amount of time needed to attend the equilibrium is nearly identical [38].

3. Results and Discussion

3.1. Spectral Analysis

Figure 1 shows the UV-Vis spectrum of the composite Ch-PANI- Fe_2O_3 material. For the Ch-PANI- Fe_2O_3 composite, the electronic transition, which demonstrates at 285–520 nm, is attributed to the ($n-\pi^*$) transition. This electronic transition is attributed to the presence of quinoid moieties of polyaniline (PANI) present in the Ch-PANI- Fe_2O_3 composite.

For chitosan, the bands appearing at 1645 and 1386 cm^{-1} are assigned to a large number of C-OH groups and C-NH₂ groups. The bands appearing at 1150–1000 cm^{-1} are assigned to a combinational vibration band associated with sugar rings. For PANI, bands appearing at 1550 cm^{-1} and 1460 cm^{-1} are assigned to quinoid ring C = C stretching and benzenoid C = C stretching [42]. For Fe_2O_3 , a band appearing at 576 cm^{-1} is attributed to Fe-O stretching [43]. For the Ch-PANI- Fe_2O_3 composite, a band appearing at 3784.53 cm^{-1} is attributed to N-H stretching vibrations. A band appearing at 1527 cm^{-1} was assigned to -C = O and N-H stretching, respectively. A band appearing at 614 cm^{-1} can be attributed to

Fe-O vibration in the Ch-PANI-Fe₂O₃ composite. FTIR spectrum and data for Ch-PANI-Fe₂O₃ are shown in Figure 2 and Table 2.

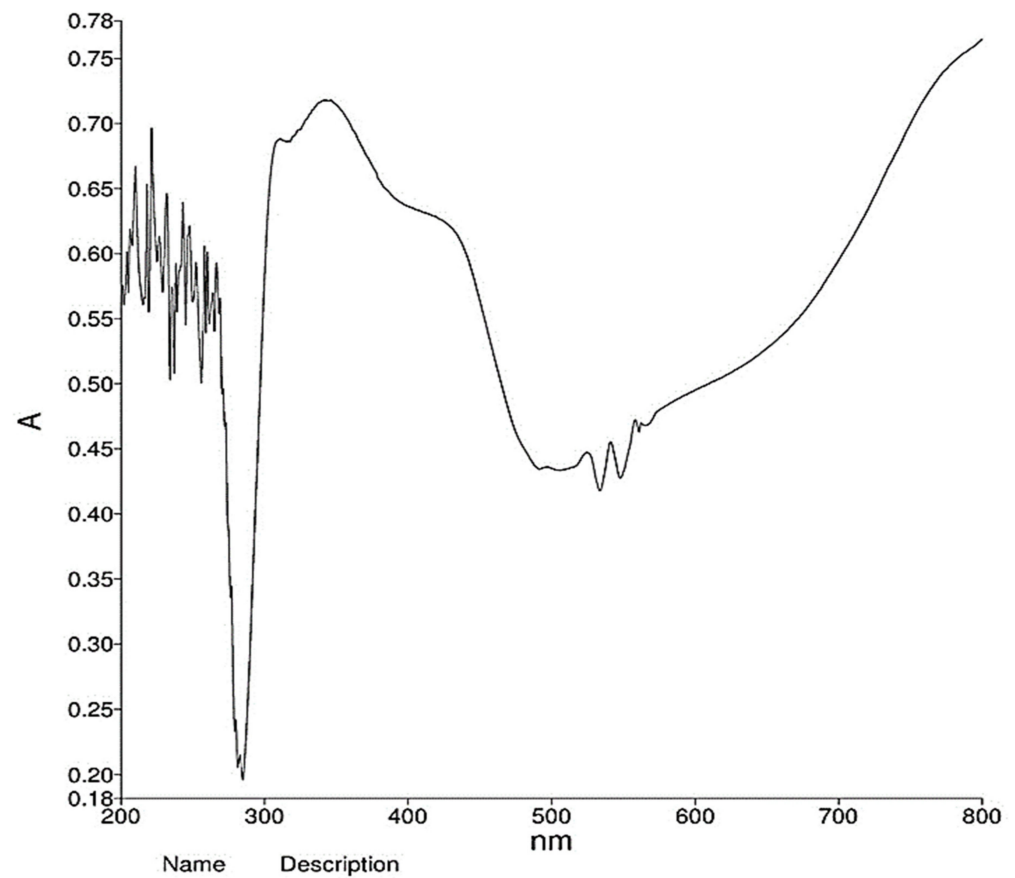


Figure 1. UV-Vis spectrum of Ch-PANI-Fe₂O₃ composite. (A) absorbance.

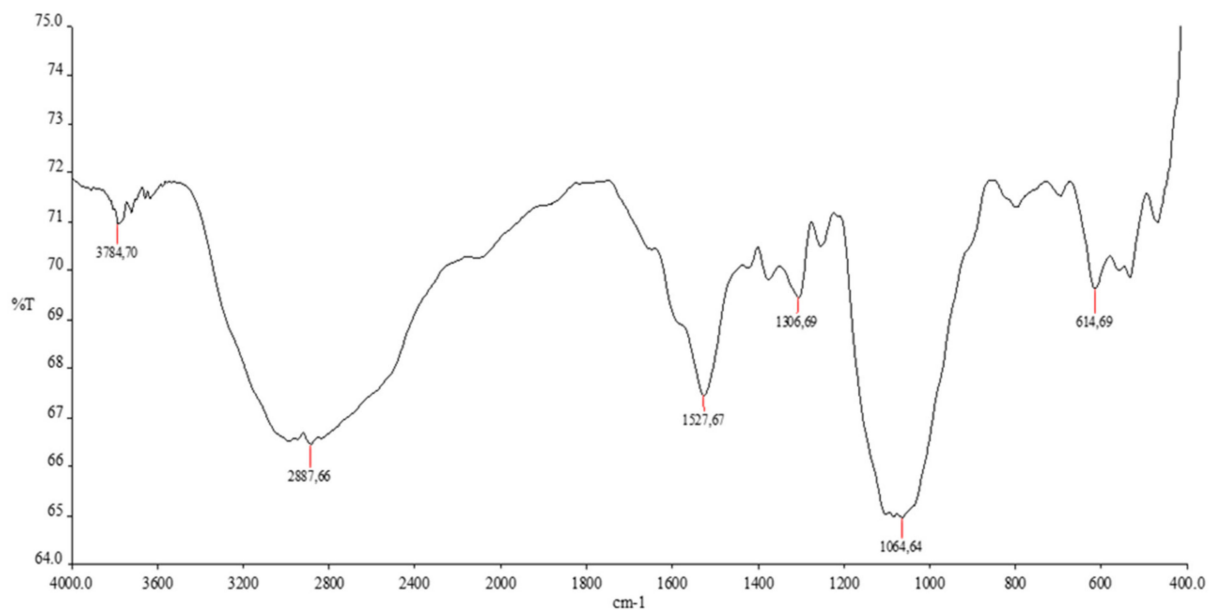


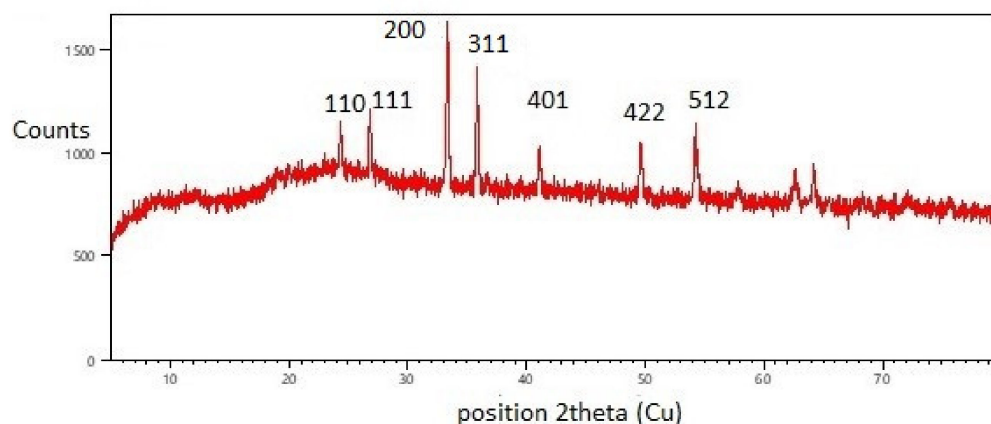
Figure 2. FTIR spectrum of Ch-PANI-Fe₂O₃ composite.

Table 2. Spectral bands of Ch-PANI-Fe₂O₃ composite.

	Bands (cm ⁻¹)	Assignments
FTIR	3784.70	O-H Stretching
	2887.66	symmetric -CH ₂ - stretching vibration credited to pyranose ring
	1527.67	-C = O and N-H stretching
	1306.69	-CH ₃ bending in alkyl-substituted amide
	1064.64	C-O stretching vibration in chitosan
	614.69	Fe-O Stretching

3.2. XRD Analysis

The XRD pattern of the Ch-PANI-Fe₂O₃ composite is given in Figure 3. It is already revealed from previously reported work that chitosan has shown broad peaks at $2\theta = 20$, for PANI at $2\theta = 20.6$ and 25.2 and Fe₂O₃ at 30.1 , 35.7 , 43.4 , 53.8 , 57.3 , 62.7 , 71.4 , and 74.5 . The observed peaks at 24.3° , 26.8° , 33.3° , 35.8° , 41.0° , 49.6° , 54.2° , 57.8° , 62.6° , 64.1° , 68.2° , 72.1° , and 75.6° are observed for the Ch-PANI-Fe₂O₃ composite, which are in good agreement with other diffraction peaks of chitosan, polyaniline, and Fe₂O₃. The particular size of the crystallites was calculated as 64.77 nm using the Debye–Scherrer formula, which is in the nanometric range.

**Figure 3.** XRD pattern of Ch-PANI-Fe₂O₃ composite.

3.3. Topographical Study

The SEM images of the Ch-PANI-Fe₂O₃ composite are shown in Figure 4. The presence of consistently packed spherically agglomerated particles were found to be sparse in some areas. In this instance, an advantage over other synthetic routes for interfacial polymerization was provided by a uniform morphology and substance homogeneity.

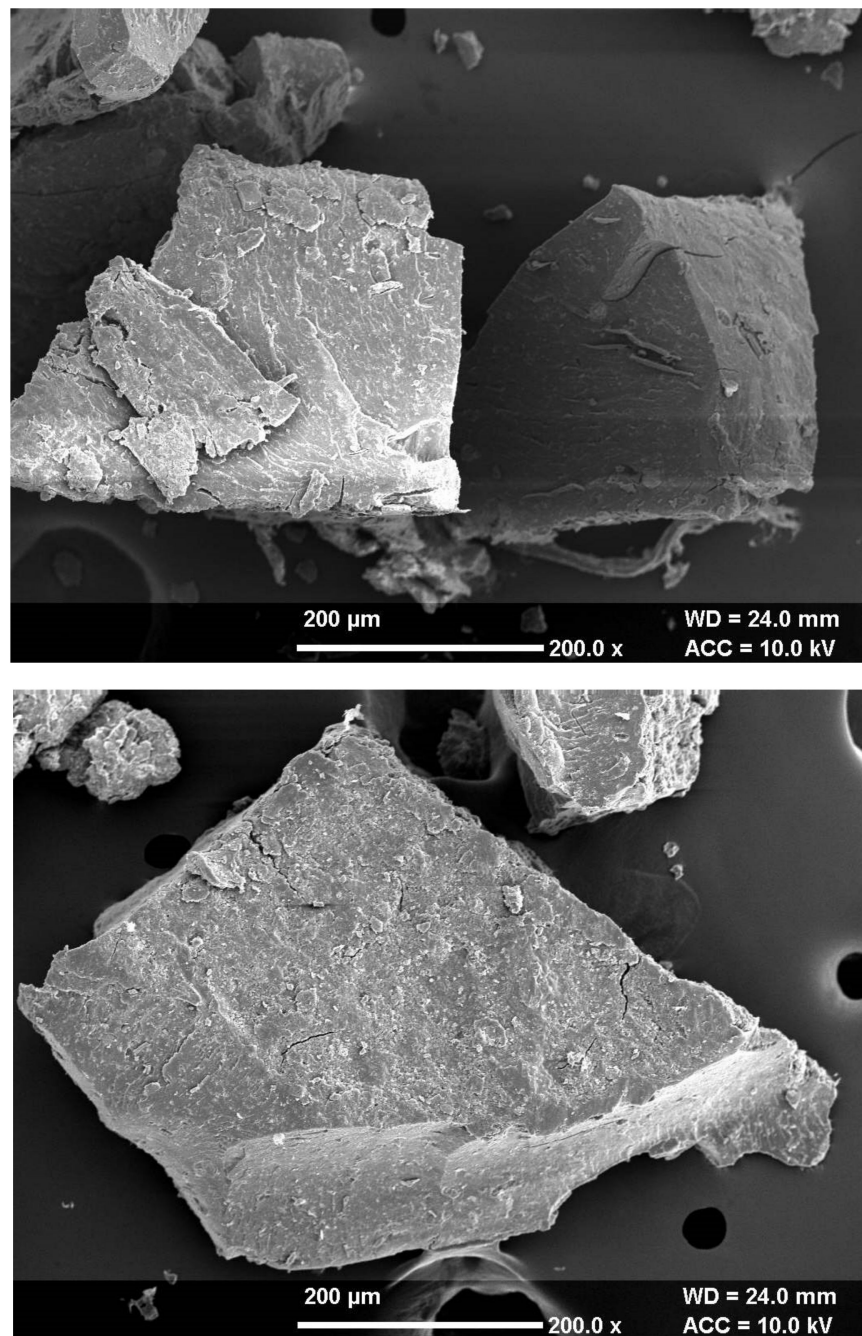
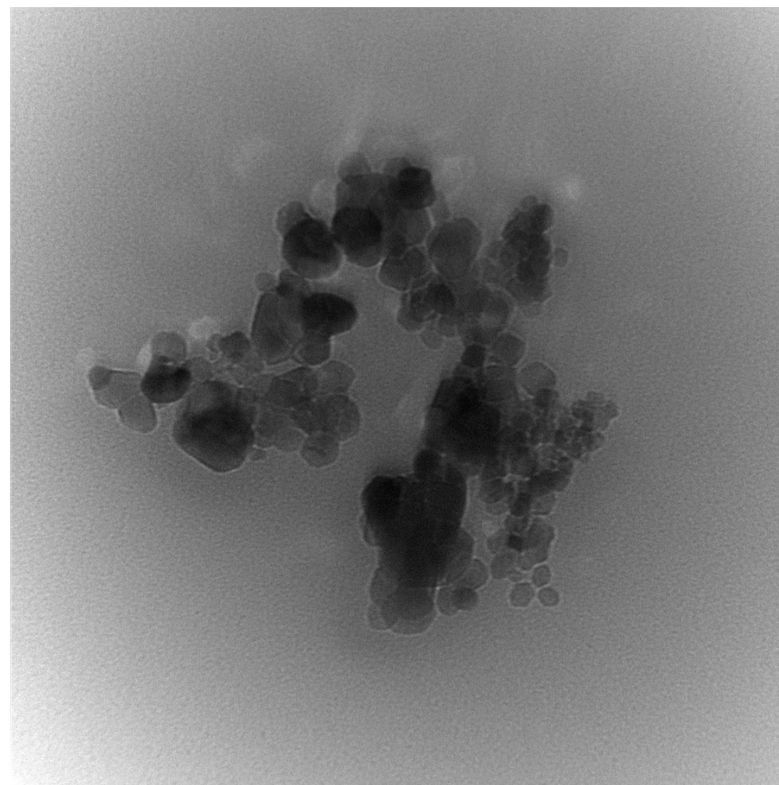


Figure 4. SEM images of Ch-PANI-Fe₂O₃ composite.

The TEM images of the Ch-PANI-Fe₂O₃ composite are presented in Figure 5. TEM images indicated that the composite had a highly dense and packed structure. Due to their high surface area and energy, Fe₂O₃ nanoparticles may have aggregated, explaining the observation of a few larger nanoparticles.



c6dr7.tif
Print Mag: 521000x @ 7.0 in
4:11:57 p 05/17/17

20 nm
HV=100.0kV
Direct Mag: 300000x
AMT Camera System



c5.tif
Print Mag: 139000x @ 7.0 in
12:21:40 p 05/18/17

100 nm
HV=100.0kV
Direct Mag: 80000x
AMT Camera System

Figure 5. TEM images of Ch-PANI-Fe₂O₃ composite.

3.4. Thermal Stability

The Ch-PANI-Fe₂O₃ composite's TG-DTG thermogram is shown in Figure 6. Three stages of weight loss were visible on the TG curve for the Ch-PANI-Fe₂O₃ composite. The first stage occurred at 50–250 °C and resulted in a weight loss of 35.99%, which corresponded to the loss of residual water from the material. The second stage involved a significant weight loss at 250–600 °C, with a total weight loss of 24.79%, which was attributable to chitosan decomposition, vaporization, and removal of volatile compounds. There is a constant weight loss of 27.73% after 650 °C up to 850 °C, which could be attributed to the dopant ion and the breakdown and disintegration of the polymer backbone. The first and second decomposition temperatures for the Ch-PANI-Fe₂O₃ composite were 205 °C and 615 °C, respectively.

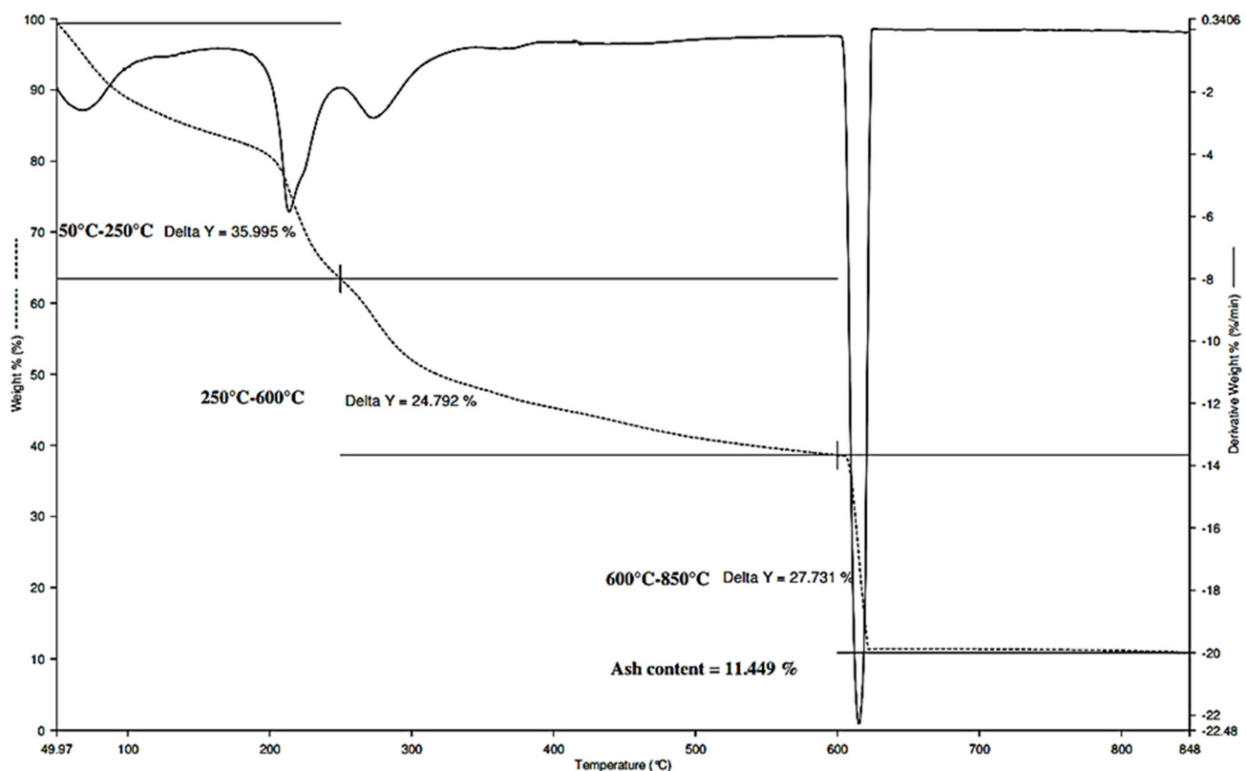
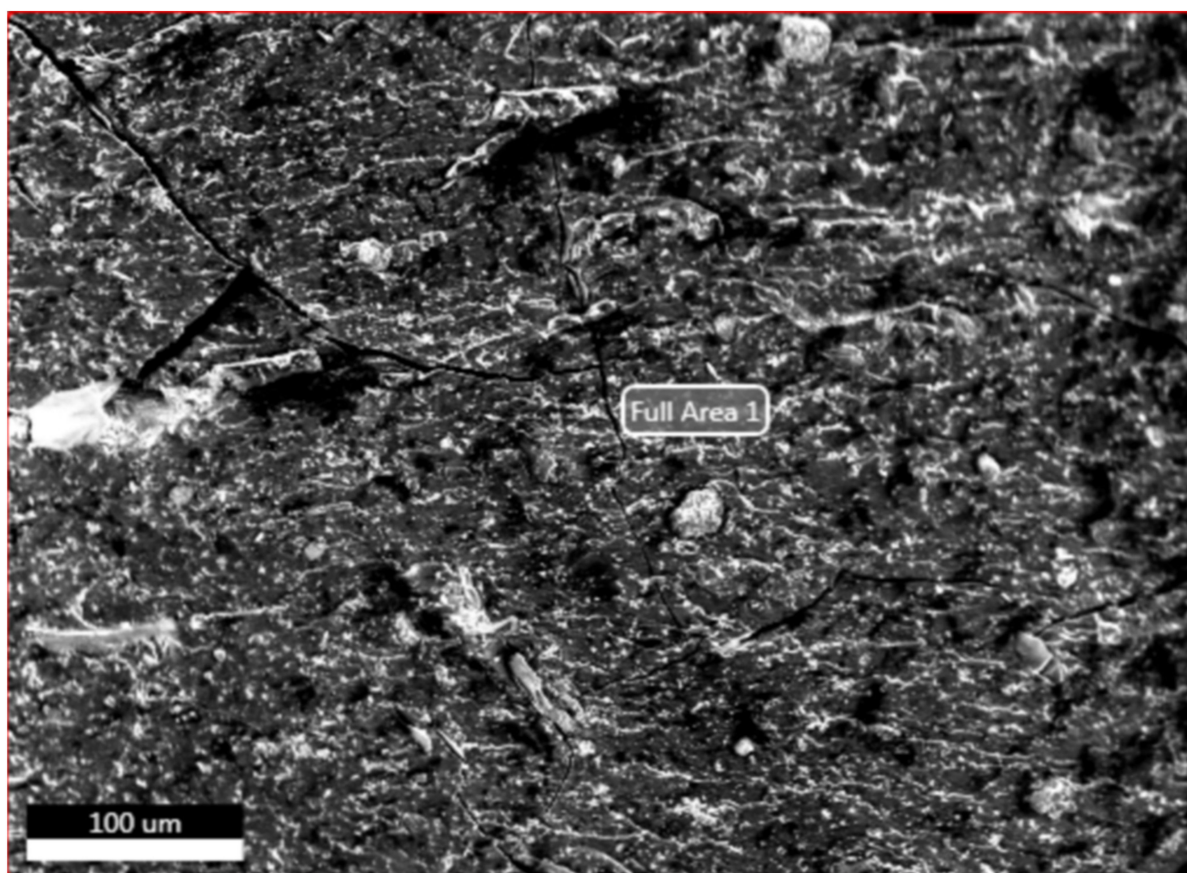


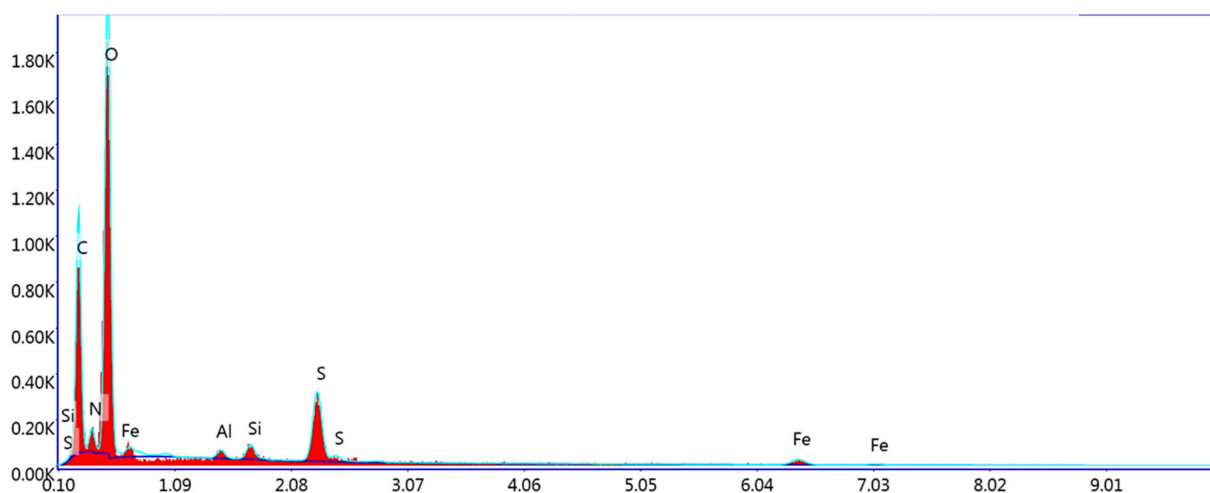
Figure 6. TG-DTG thermogram for Ch-PANI-Fe₂O₃ composite.

3.5. Elemental Analysis

In Figure 7a, the morphological characteristics of the hybrid Ch-PANI-Fe₂O₃ composite that underwent SEM investigation are displayed. The Fe₂O₃ nanoparticle integration into the chitosan–polyaniline matrix has uniform granular porosity shape, which is attributable to the homogeneous dispersion of Fe₂O₃ nanoparticles in the chitosan–polyaniline matrix, as demonstrated in Figure 7b according to the SEM-EDX of the Ch-PANI-Fe₂O₃ hybrid composite. The elements that were present in the hybrid composite were examined. Figure 4 displays the SEM-EDX spectrum at various places. It displays peaks at 0.22, 0.38, and 0.56 keV for selected region 1, which correspond to carbon, nitrogen, and oxygen, respectively. The peaks seen at 0.65, 6.44, and 7.04 are due to the presence of Fe. The weight ratios of the Ch-PANI-Fe₂O₃ hybrid composite, as determined by EDX, are as follows: C 34.25%; N 00.48%; O 50.51%; and Fe 3.08%. Thus, it is evident that C, N, O, and Fe are present, proving that the hybrid composites contain both polymer and Fe₂O₃.



(a)



(b)

Figure 7. (a) SEM image and (b) EDX analysis at selected area 1.

3.6. Dye Adsorption Study

The initial concentrations of the methyl orange dye affected how rapidly it was eliminated. The rapid transport of the dye into the activated site of the composite may be the reason for the improved elimination of the methyl orange at the low concentration. The rate of elimination was slowed down at increasing dye concentrations. This might be the result of steric attraction between the solid particles and intraparticle diffusion, which allows dye molecules to diffuse onto the site of the adsorbent. Using agricultural waste, Hameed was able to remove the methyl violet with results that were comparable [44].

The amount of adsorbent used is a crucial component in controlling the adsorption of hazardous dyes during the treatment of wastewater. The increasing adsorption active site on the adsorbent surface may account for the increasing removal effectiveness of methyl orange with increasing adsorbent dosage. The remarkable removal effectiveness with a comparatively small dosage of nanocomposite demonstrates its good affinity and stability for the elimination of methyl orange from aqueous solution. There is no noticeable difference in removal efficiency for the composite concentration from 0.1 to 0.5 g L⁻¹ due to the concentration gradient between the methyl orange and the adsorbent surface. The amount of methyl orange adsorbed onto the unit weight of adsorbent thus decreases as adsorbent dosages are increased [45].

3.6.1. Effect of pH

In the pH range 3.0–12.0, the effect of pH on removal efficiency was observed. The pH of the medium was adjusted with a decimolar solution of hydrochloric and sodium hydroxide. The results are reported graphically in Figure 8. It has been noted that dye removal efficiency was maximum at pH = 5. This is attributed to the higher quantity of dye adsorbed and the protonation of relatively more nitrogen atoms present on the chitosan and polyaniline, and also attributed to the bigger surface area of Fe₂O₃. In the alkaline range, hydroxide ions may compete effectively with the anionic part of dye, which results in a decrease in the efficiency of dye removal.

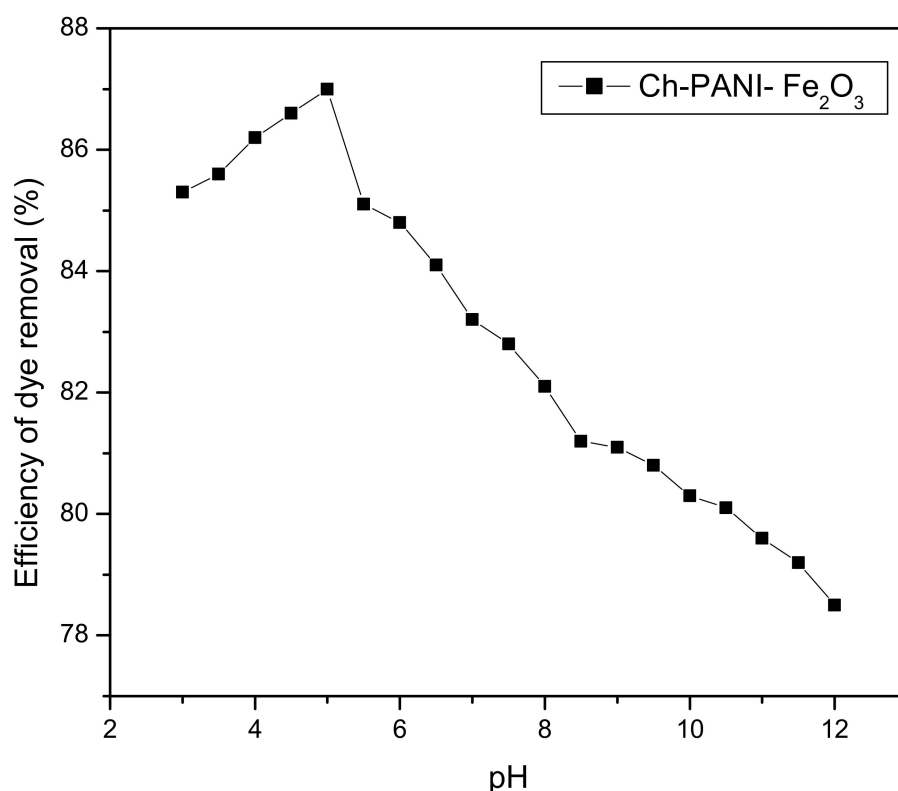


Figure 8. A plot between pH and dye removal efficiency for Ch-PANI-Fe₂O₃ composite.

Adsorption was significantly influenced by pH. The degree of ionization of the substances in solution, as well as the various functional groups present on the adsorbent, are all influenced by the pH of the solution. This hybrid material is a strong candidate to remove the colors from the effluent because of its low cost and high removal rate. Additionally, the impact of pH on dye adsorption at a range of pH values from 3 to 12 was investigated. It was revealed that the dye was most effectively removed at a particular pH, especially in the acidic range. The presence of an abundance of OH ions and deprotonation of the

functional group, which increased the electrostatic repulsion between the adsorbent and adsorbate, may explain the low adsorption found in the pH range of 6–9. This is because protonation of functional groups prevents electrostatic attraction between the positively charged adsorbent surface and neutral dye molecule. The adsorption of an anionic dye molecule is inhibited by a negatively charged surface on the adsorbent dosage. This hybrid material was a strong candidate to remove the dyes from the wastewater because of its low cost and high removal rate.

3.6.2. Effect of Dose of Adsorbent and Dye

The amount of adsorbent used is a crucial component in controlling the adsorption of hazardous dyes during the treatment of wastewater. The increased adsorption active site on the adsorbent surface may account for the increasing removal efficacy of methyl orange with increasing adsorbent dosage. The remarkable removal effectiveness at a relatively modest dosage of nanocomposite suggests that it has a high affinity and stability for removing methyl orange from an aqueous solution. Due to the concentration gradient between the methyl orange and adsorbent surface, the removal efficiency for the composite concentration does not change significantly from 0.1 to 0.5 g L⁻¹. The amount of methyl orange adsorbed onto the unit weight of adsorbent thus decreases as adsorbent dosages are increased [16,45].

For three concentrations (0.1, 0.25, and 0.5 mg L⁻¹), the influence of adsorbent concentration on the efficiency of dye removal was studied. The results are summarized in Table 3 and shown in Figure 9.

Table 3. Different concentrations and efficiency of dye removal for Ch-PANI-Fe₂O₃ composite.

Time (min)	Ch-PANI-Fe ₂ O ₃ (0.1 mg L ⁻¹)	Ch-PANI-Fe ₂ O ₃ (0.25 mg L ⁻¹)	Ch-PANI-Fe ₂ O ₃ (0.5 mg L ⁻¹)
0.0	0.0	0.0	0.0
5.0	81.2	84.3	88.2
10.0	81.6	84.4	88.7
15.0	81.9	85.1	89.2
20.0	82.5	85.3	89.9
25.0	83.0	85.9	90.3
30.0	83.7	86.7	90.5
35.0	83.9	87.0	90.8
40.0	84.1	87.3	91.5
45.0	84.5	88.2	92.4
50.0	84.9	88.6	93.5
55.0	85.3	89.2	93.8
60.0	85.6	89.5	94.3

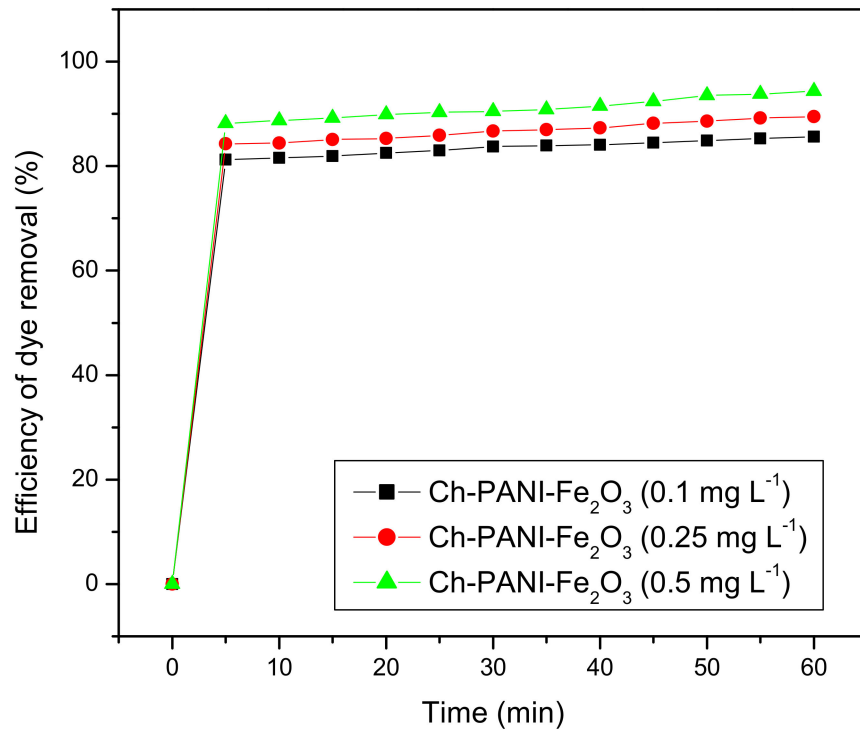


Figure 9. Dye removal efficiency at fixed amounts for Ch-PANI-Fe₂O₃ composite.

The dye concentrations regarding removal efficiency were studied in the range of 20.0–100 mg L⁻¹. The results are graphically presented in Figure 10.

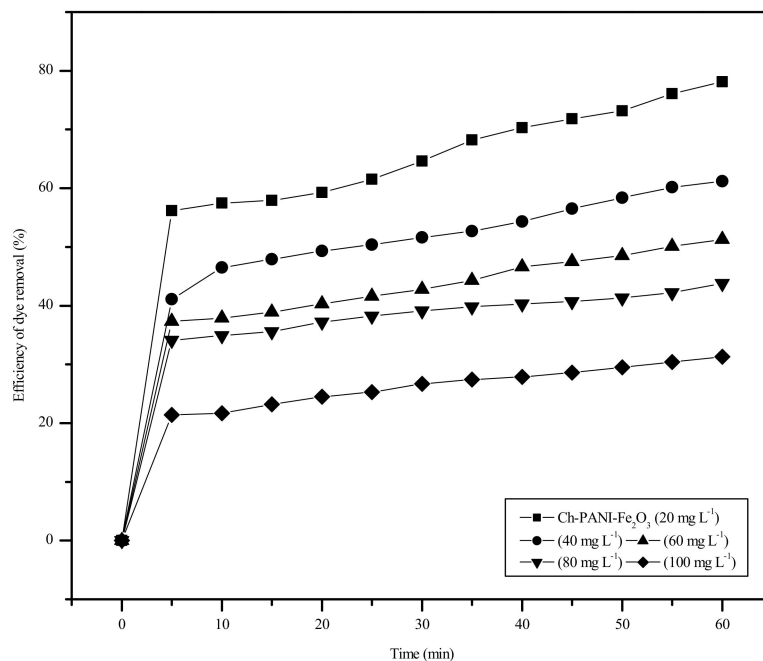


Figure 10. Variation in efficiency of dye removal using Ch-PANI- Fe₂O₃ composite at different dye concentrations.

3.6.3. Effect of Wavelength

The effect on absorbance with different wavelength ranges (385–500 nm) was observed for the Ch-PANI- Fe₂O₃ composite and is depicted in Figure 11. The absorbance is maximum (0.601) at a wavelength of 465 nm.

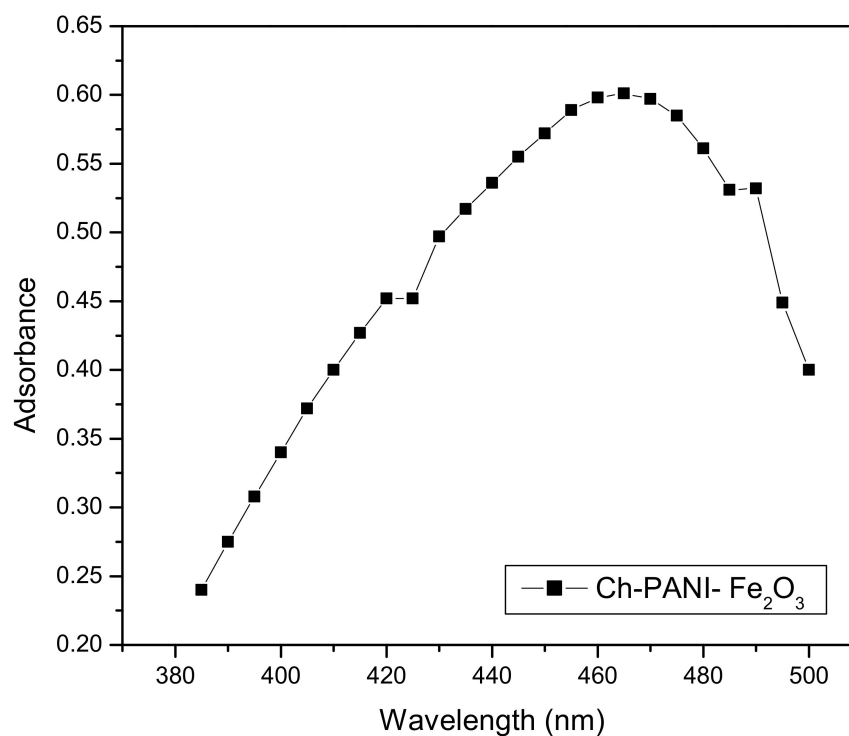


Figure 11. A plot of wavelength and absorbance of Ch-PANI- Fe_2O_3 composite.

3.6.4. Photocatalytic Activity

To understand the impact of irradiation on catalyst dye interaction, the photocatalytic activity of composite materials was investigated. This was achieved in two sets of experiments. The first set involved the removal of dye under dark conditions while a catalyst was present, whereas the second set was carried out when light irradiation was present.

The removal of dye in the presence of the Ch-PANI- Fe_2O_3 composite (in light and dark) is reported graphically in Figure 12.

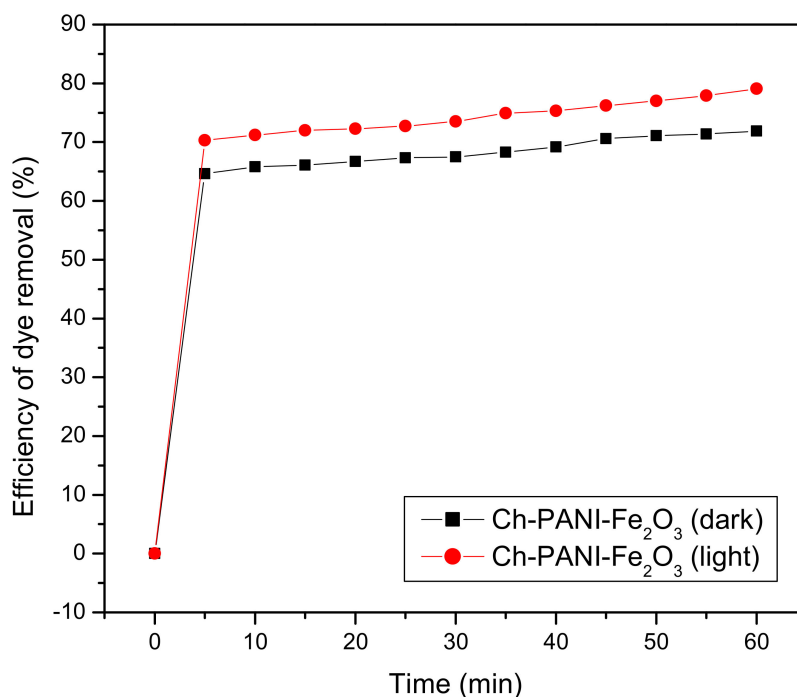


Figure 12. Plot of time and efficiency of dye removal for Ch-PANI- Fe_2O_3 composite.

Initial MO dye adsorption occurs rapidly, followed by relatively slow adsorption that takes place over time as it approaches equilibrium. The results indicate that the Ch-PANI-Fe₂O₃ hybrid's surface, which contains highly concentrated active binding sites, is where adsorption initially takes place most frequently, leading to a fast adsorption rate. As free sites are gradually occupied until saturation, adsorption slowly moves into the interior of the hybrid through the diffusion of MO, resulting in a lower adsorption rate. The duration needed to reach equilibrium is referred to as the equilibrium time, and the amount of MO adsorbed at equilibrium time reflects the adsorption capacity of the adsorbent under these specific circumstances. All of these findings indicate that the enthalpy of the adsorption would be reduced through coulombic interactions, hydrogen bonds, and π - π stacking.

4. Conclusions

A combination of analytical methods, including FTIR, UV-visible, SEM, TEM, EDX, TG-DTG, and XRD, were used to characterize the composites made from the synthesis of a Ch-PANI composite and Ch-PANI-Fe₂O₃ nanocomposites in the presence of acetic acid. Batch experiments were used to evaluate the adsorption of methyl orange on the Ch-PANI composite as a function of the adsorbate concentration, the dose of the adsorbent, and the pH of the solution. The dye adsorption efficiency for the Ch-PANI-Fe₂O₃ composite was found to be 91.5%. Thus, the composite can be successfully utilized to remove methyl orange from industrial contaminated water, and in this way it will find wider application in the allied fields of material science such as water purification.

Author Contributions: Conceptualization, B.S.R. and N.P.S.C.; methodology, N.P.S.C. and R.A. software, S.J.; validation, P.P., M.B., S.C.A. and R.A.; formal analysis, P.P.; investigation, B.S.R.; resources, M.B.; data curation, B.S.R. and P.P.; writing—original draft preparation, B.S.R., N.P.S.C., P.P., S.J. and M.B.; writing—review and editing, M.B., N.P.S.C. and R.A.; visualization, B.S.R.; supervision, N.P.S.C., R.A. and S.C.A.; project administration, M.B., P.P. and R.A.; funding acquisition, M.B. All authors have read and agreed to the published version of the manuscript.

Funding: This research received no external funding.

Data Availability Statement: Not applicable.

Conflicts of Interest: The authors declare no conflict of interest.

References

1. Sabbagh, F.; Kiarostami, K.; Khatir, N.M.; Rezanian, S.; Muhamad, I.I.; Hosseini, F. Effect of zinc content on structural, functional, morphological, and thermal properties of kappa-carrageenan/NaCMC nanocomposites. *Polym. Test.* **2021**, *93*, 106922. [[CrossRef](#)]
2. Chen, F.; Ma, J.; Zhu, Y.; Li, X.; Yu, H.; Sun, Y. Biodegradation performance and anti-fouling mechanism of an ICME/electro-biocarriers-MBR system in livestock wastewater (antibiotic-containing) treatment. *J. Hazard. Mater.* **2022**, *426*, 128064. [[CrossRef](#)]
3. Wan, Z.; Zhang, T.; Liu, Y.; Liu, P.; Zhang, J.; Fang, L.; Sun, D. Enhancement of desulfurization by hydroxyl ammonium ionic liquid supported on active carbon. *Environ. Res.* **2022**, *213*, 113637. [[CrossRef](#)] [[PubMed](#)]
4. Ramakrishna, K.R.; Viraraghavan, T. Dye removal using low cost adsorbents. *Water Sci. Technol.* **1997**, *36*, 189–196. [[CrossRef](#)]
5. Shindhal, T.; Rakholiya, P.; Varjani, S.; Pandey, A.; Ngo, H.H.; Guo, W.; Ng, H.Y.; Taherzadeh, M.J. A critical review on advances in the practices and perspectives for the treatment of dye industry wastewater. *Bioengineered* **2021**, *12*, 70–87. [[CrossRef](#)] [[PubMed](#)]
6. Liu, W.; Huang, F.; Liao, Y.; Zhang, J.; Ren, G.; Zhuang, Z.; Zhen, J.; Lin, Z.; Wang, C. Treatment of CrVI-Containing Mg(OH)₂ Nanowaste. *Angew. Chem.* **2008**, *120*, 5701–5704. [[CrossRef](#)]
7. Tian, Y.; Yang, Z.; Yu, X.; Jia, Z.; Rosso, M.; Dedman, S.; Zhu, J.; Xia, Y.; Zhang, G.; Yang, J. Can we quantify the aquatic environmental plastic load from aquaculture? *Water Res.* **2022**, *219*, 118551. [[CrossRef](#)]
8. Madhu, N.R.; Erfani, H.; Jadoun, S.; Amir, M.; Thiagarajan, Y.; Chauhan, N.P.S. Fused deposition modelling approach using 3D printing and recycled industrial materials for a sustainable environment: A review. *Int. J. Adv. Manuf. Technol.* **2022**, *122*, 2125–2138. [[CrossRef](#)]
9. Weisburger, J.H. Comments on the history and importance of aromatic and heterocyclic amines in public health. *Mutat. Res. Fundam. Mol. Mech. Mutagen.* **2002**, *506*, 9–20. [[CrossRef](#)]
10. Shabani-Nooshabadi, M.; Roostaei, M. Coupling of NiO nanoparticles and room temperature ionic liquid for fabrication of highly sensitive voltammetric sensor in tryptophan analysis. *Anal. Bioanal. Electrochem.* **2016**, *8*, 578–588.

11. Mortezaigholi, B.; Movahed, E.; Fathi, A.; Soleimani, M.; Forutan Mirhosseini, A.; Zeini, N.; Khatami, M.; Naderifar, M.; Abedi Kiasari, B.; Zareanshahraki, M. Plant-mediated synthesis of silver-doped zinc oxide nanoparticles and evaluation of their antimicrobial activity against bacteria cause tooth decay. *Microsc. Res. Tech.* **2022**, *85*, 3553–3564. [[CrossRef](#)] [[PubMed](#)]
12. Akbarizadeh, M.R.; Naderifar, M.; Mousazadeh, F.; Zafarnia, N.; Sarani, M. Cytotoxic activity and Magnetic Behavior of green synthesized iron oxide nanoparticles on brain glioblastoma cells. *Nanomed. Res. J.* **2022**, *7*, 99–106.
13. Kalal, S.; Singh Chauhan, N.P.; Ameta, N.; Ameta, R.; Kumar, S.; Punjabi, P.B. Role of copper pyrovanadate as heterogeneous photo-Fenton like catalyst for the degradation of neutral red and azure-B: An eco-friendly approach. *Korean J. Chem. Eng.* **2014**, *31*, 2183–2191. [[CrossRef](#)]
14. Anuma, S.; Mishra, P.; Bhat, B.R. Polypyrrole functionalized Cobalt oxide Graphene (COPYGO) nanocomposite for the efficient removal of dyes and heavy metal pollutants from aqueous effluents. *J. Hazard. Mater.* **2021**, *416*, 125929. [[CrossRef](#)] [[PubMed](#)]
15. Raghunath, S.; Anand, K.; Gengan, R.M.; Nayunigari, M.K.; Maity, A. Sorption isotherms, kinetic and optimization process of amino acid proline based polymer nanocomposite for the removal of selected textile dyes from industrial wastewater. *J. Photochem. Photobiol. B Biol.* **2016**, *165*, 189–201. [[CrossRef](#)] [[PubMed](#)]
16. Shukla, A.K.; Alam, J.; Rahaman, M.; Alrehaili, A.; Alhoshan, M.; Aldalbahi, A. A facile approach for elimination of electroneutral/anionic organic dyes from water using a developed carbon-based polymer nanocomposite membrane. *Water Air Soil Pollut.* **2020**, *231*, 104. [[CrossRef](#)]
17. Jagadish, K.; Chandrashekar, B.; Byrappa, K.; Rangappa, K.; Srikantaswamy, S. Simultaneous removal of dye and heavy metals in a single step reaction using PVA/MWCNT composites. *Anal. Methods* **2016**, *8*, 2408–2412. [[CrossRef](#)]
18. Eltaweil, A.S.; Abd El-Monaem, E.M.; El-Subruiti, G.M.; Abd El-Latif, M.M.; Omer, A.M. Fabrication of UiO-66/MIL-101 (Fe) binary MOF/carboxylated-GO composite for adsorptive removal of methylene blue dye from aqueous solutions. *RSC Adv.* **2020**, *10*, 19008–19019. [[CrossRef](#)]
19. Chen, B.; Liu, Y.; Chen, S.; Zhao, X.; Meng, X.; Pan, X. Magnetically recoverable cross-linked polyethylenimine as a novel adsorbent for removal of anionic dyes with different structures from aqueous solution. *J. Taiwan Inst. Chem. Eng.* **2016**, *67*, 191–201. [[CrossRef](#)]
20. Cojocar, C.; Samoila, P.; Pascariu, P. Chitosan-based magnetic adsorbent for removal of water-soluble anionic dye: Artificial neural network modeling and molecular docking insights. *Int. J. Biol. Macromol.* **2019**, *123*, 587–599. [[CrossRef](#)]
21. Jadoun, S.; Rathore, D.S.; Riaz, U.; Chauhan, N.P.S. Tailoring of conducting polymers via copolymerization—A review. *Eur. Polym. J.* **2021**, *155*, 110561. [[CrossRef](#)]
22. Chauhan, N.P.; Ameta, R.; Ameta, R.; Ameta, S.C. Thermal and conducting behaviour of emeraldine base (EB) form of polyaniline (PANI). *Indian J. Chem. Technol.* **2011**, *18*, 118–122.
23. Mozafari, M.; Chauhan, N.P.S. *Fundamentals and Emerging Applications of Polyaniline*; Elsevier: Amsterdam, The Netherlands, 2019.
24. Supriya, S.; Palanisamy, P. Adsorptive removal of acid orange 7 from industrial effluents using activated carbon and conducting polymer composite—A comparative study. *Indian J. Chem. Technol.* **2016**, *23*, 506–512.
25. Abbasian, M.; Niroomand, P.; Jaymand, M. Cellulose/polyaniline derivatives nanocomposites: Synthesis and their performance in removal of anionic dyes from simulated industrial effluents. *J. Appl. Polym. Sci.* **2017**, *134*, 45352. [[CrossRef](#)]
26. Wang, N.; Chen, J.; Wang, J.; Feng, J.; Yan, W. Removal of methylene blue by Polyaniline/TiO₂ hydrate: Adsorption kinetic, isotherm and mechanism studies. *Powder Technol.* **2019**, *347*, 93–102. [[CrossRef](#)]
27. Muhammad, A.; Shah, A.U.H.A.; Bilal, S. Comparative study of the adsorption of Acid Blue 40 on polyaniline, magnetic oxide and their composites: Synthesis, characterization and application. *Materials* **2019**, *12*, 2854. [[CrossRef](#)] [[PubMed](#)]
28. Kumar, M.N.R. A review of chitin and chitosan applications. *React. Funct. Polym.* **2000**, *46*, 1–27. [[CrossRef](#)]
29. AlYahya, S.; Rani, B.J.; Ravi, G.; Yuvakkumar, R.; Arun, A.; Ameen, F.; AlNadhary, S. Size dependent magnetic and antibacterial properties of solvothermally synthesized cuprous oxide (Cu₂O) nanocubes. *J. Mater. Sci. Mater. Electron.* **2018**, *29*, 17622–17629. [[CrossRef](#)]
30. Swathi, S.; Ameen, F.; Ravi, G.; Yuvakkumar, R.; Hong, S.; Velauthapillai, D.; AlKahtani, M.D.; Thambidurai, M.; Dang, C. Cancer targeting potential of bioinspired chain like magnetite (Fe₃O₄) nanostructures. *Curr. Appl. Phys.* **2020**, *20*, 982–987. [[CrossRef](#)]
31. Jasni, M.; Sathishkumar, P.; Sornambikai, S.; Yusoff, A.R.M.; Ameen, F.; Buang, N.A.; Kadir, M.R.A.; Yusop, Z. Fabrication, characterization and application of laccase-nylon 6, 6/Fe³⁺ composite nanofibrous membrane for 3, 3'-dimethoxybenzidine detoxification. *Bioprocess Biosyst. Eng.* **2017**, *40*, 191–200. [[CrossRef](#)]
32. Hu, X.; Derakhshanfard, A.H.; Khalid, I.; Jalil, A.T.; Opulencia, M.J.C.; Dehkordi, R.B.; Toghraie, D.; Hekmatifar, M.; Sabetvand, R. The microchannel type effects on water-Fe₃O₄ nanofluid atomic behavior: Molecular dynamics approach. *J. Taiwan Inst. Chem. Eng.* **2022**, *135*, 104396. [[CrossRef](#)]
33. Homaeigohar, S. The nanosized dye adsorbents for water treatment. *Nanomaterials* **2020**, *10*, 295. [[CrossRef](#)] [[PubMed](#)]
34. Roostae, M.; Sheikhshoae, I. Fabrication of a sensitive sensor for determination of xanthine in the presence of uric acid and ascorbic acid by modifying a carbon paste sensor with Fe₃O₄@Au core-shell and an ionic liquid. *J. Food Meas. Charact.* **2022**, *16*, 731–739. [[CrossRef](#)]
35. Pandiselvi, K.; Thambidurai, S. Synthesis of adsorption cum photocatalytic nature of polyaniline-ZnO/chitosan composite for removal of textile dyes. *Desalination Water Treat.* **2016**, *57*, 8343–8357. [[CrossRef](#)]
36. Kannusamy, P.; Sivalingam, T. Chitosan-ZnO/polyaniline hybrid composites: Polymerization of aniline with chitosan-ZnO for better thermal and electrical property. *Polym. Degrad. Stab.* **2013**, *98*, 988–996. [[CrossRef](#)]

37. Shahabuddin, S.; Sarih, N.M.; Ismail, F.H.; Shahid, M.M.; Huang, N.M. Synthesis of chitosan grafted-polyaniline/ Co_3O_4 nanocube nanocomposites and their photocatalytic activity toward methylene blue dye degradation. *RSC Adv.* **2015**, *5*, 83857–83867. [[CrossRef](#)]
38. Kannusamy, P.; Sivalingam, T. Synthesis of porous chitosan–polyaniline/ ZnO hybrid composite and application for removal of reactive orange 16 dye. *Colloids Surf. B: Biointerfaces* **2013**, *108*, 229–238. [[CrossRef](#)]
39. Vellakkat, M.; Hundekal, D. Electrical conductivity and supercapacitor properties of polyaniline/chitosan/nickel oxide honeycomb nanocomposite. *J. Appl. Polym. Sci.* **2017**, *134*, 44536. [[CrossRef](#)]
40. Rathore, B.S.; Chauhan, N.P.S.; Jadoun, S.; Ameta, S.C.; Ameta, R. Synthesis and characterization of chitosan-polyaniline-nickel (II) oxide nanocomposite. *J. Mol. Struct.* **2021**, *1242*, 130750. [[CrossRef](#)]
41. Mahanta, D.; Madras, G.; Radhakrishnan, S.; Patil, S. Adsorption and desorption kinetics of anionic dyes on doped polyaniline. *J. Phys. Chem. B* **2009**, *113*, 2293–2299. [[CrossRef](#)]
42. Rathore, B.S.; Chauhan, N.P.S.; Rawal, M.K.; Ameta, S.C.; Ameta, R. Chitosan–polyaniline–copper (II) oxide hybrid composite for the removal of methyl orange dye. *Polym. Bull.* **2020**, *77*, 4833–4850. [[CrossRef](#)]
43. Farahmandjou, M.; Soflaee, F. Synthesis and characterization of $\alpha\text{-Fe}_2\text{O}_3$ nanoparticles by simple co-precipitation method. *Phys. Chem. Res.* **2015**, *3*, 191–196.
44. Hameed, B. Equilibrium and kinetic studies of methyl violet sorption by agricultural waste. *J. Hazard. Mater.* **2008**, *154*, 204–212. [[CrossRef](#)] [[PubMed](#)]
45. Dawood, S.; Sen, T.K. Removal of anionic dye Congo red from aqueous solution by raw pine and acid-treated pine cone powder as adsorbent: Equilibrium, thermodynamic, kinetics, mechanism and process design. *Water Res.* **2012**, *46*, 1933–1946. [[CrossRef](#)]